To appear in The Astrophysical Journal, March 10, 2001
Preprint typeset using LaTeX style emulateapj v. 14/09/00

THE SEYFERT-STARBURST CONNECTION IN X-RAYS. II. RESULTS AND IMPLICATIONS

N. A. Levenson, K. A. Weaver[1], and T. M. Heckman
Department of Physics and Astronomy, Bloomberg Center, Johns Hopkins University, Baltimore, MD 21218
To appear in The Astrophysical Journal, March 10, 2001

ABSTRACT

We present the results of X-ray imaging and spectroscopic analysis of a sample of Seyfert 2 galaxies that contain starbursts, based on their optical and UV characteristics. These composite galaxies exhibit extended, soft, thermal X-ray emission, which we attribute to their starburst components. Comparing their X-ray and far-infrared properties with ordinary Seyfert and starburst galaxies, we identify the spectral characteristics of their various intrinsic emission sources. The observed far-infrared emission of the composite galaxies may be associated almost exclusively with star formation, rather than the active nucleus. The ratio of the hard X-ray luminosity to the far-infrared and [O III] λ5007 luminosity distinguishes most of these composite galaxies from "pure" Seyfert 2 galaxies, while their total observed hard X-ray luminosity distinguishes them from "pure" starbursts. The hard nuclear X-ray source is generally heavily absorbed ($N_H > 10^{23}\,\mathrm{cm}^{-2}$) in the composite galaxies. Based on these results, we suggest that the interstellar medium of the nuclear starburst is a significant source of absorption. The majority of the sample are located in groups or are interacting with other galaxies, which may trigger the starburst or allow rapid mass infall to the central black hole, or both. We conclude that starbursts are energetically important in a significant fraction of active galaxies, and starbursts and active galactic nuclei may be part of a common evolutionary sequence.

Subject headings: galaxies: Seyfert — X-rays: galaxies

1. SEYFERT AND STARBURST GALAXIES

One of the major goals of astrophysics is to elucidate the physical processes that drove the strong cosmic evolution of the active galactic nucleus (AGN) and galaxy populations. The apparent ubiquity of supermassive black holes in the nuclei of present-day galaxies and the strong correlation between the mass of the black hole and the velocity dispersion of its "host" stellar spheroid (Ferrarese & Merritt 2000; Gebhardt et al. 2000) implies that the creation of supermassive black holes (presumably corresponding to a luminous QSO phase) was an integral part of the formation of ellipticals and galactic bulges. Thus, understanding the "starburst-AGN connection" is a crucial component of modern cosmogony.

Directly studying the starburst-AGN connection at high redshift is hard. The limitations on spatial resolution and signal-to-noise make it very difficult to use imaging or spectroscopy to disentangle processes due to the starburst or AGN, or to try to separate cause from effect. Thus, very little is known about the possible role of starbursts in typical high-redshift QSOs (cf. Ridgway et al. 2000), about AGNs in the "Lyman Break" population of star-forming galaxies (e.g., Adelberger & Steidel 2000), about the relative energetic importance of star-formation and AGN in high-redshift sub-mm sources (e.g., Barger, Cowie, & Richards 2000), or about the nature of the optically-faint (presumably distant) contributors to the cosmic X-ray background that *Chandra* has recently discovered (Mushotzky et al. 2000; Hornschemeier et al. 2000; Giacconi et al. 2000).

Fortunately, we have some excellent local laboratories in which the starburst-AGN connection can be probed in considerably more detail. The most powerful AGNs near enough to study in such detail are the Seyfert galaxies. The type 2 Seyferts are particularly well-suited to such investigations because the bright glare from the central engine has been providentially blocked by the high gas and dust column density of an "obscuring torus". Indeed, while a standard AGN model of accretion onto supermassive black holes generally describes the central engines of many Seyfert galaxies successfully (e.g., Miyoshi et al. 1995; Tanaka et al. 1995, and Nandra et al. 1997), starbursts are also significant, often in the same galaxies.

To address these issues, we are specifically examining the X-ray properties of a sample of Sy 2 galaxies that definitely contain starbursts, the Sy2/SB composite galaxies. We present the data and detailed analysis separately (Levenson, Weaver, & Heckman 2000; Paper I) and in this work concentrate on the relationship of these results to the broader questions of the Seyfert-starburst connection. We summarize the physical characteristics derived from the spatial and spectral modelling of the sample in §2 and present general results in §3. We discuss the X-ray properties of this sample and compare them with other samples in §4, and we summarize our conclusions in §5.

2. DATA AND MODELS

The present sample is selected from the optical and radio flux-limited sample of Heckman et al. (1995). This larger sample contains the 30 brightest Seyfert 2 nuclei based on [O III] $\lambda\lambda 4959 + 5007$ emission line flux and nuclear nonthermal monochromatic flux (νF_ν) at 1.4 GHz from the compilation of Whittle (1992). Members of the Heckman et al. (1995) sample have either $\log F_{[\mathrm{OIII}]} \geq -12.0\,\mathrm{erg\,cm^{-2}\,s^{-1}}$, or $\log F_{1.4} \geq -15.0\,\mathrm{erg\,cm^{-2}\,s^{-1}}$, or

[1] Laboratory for High Energy Astrophysics, Code 662, NASA/GSFC, Greenbelt, MD 20771

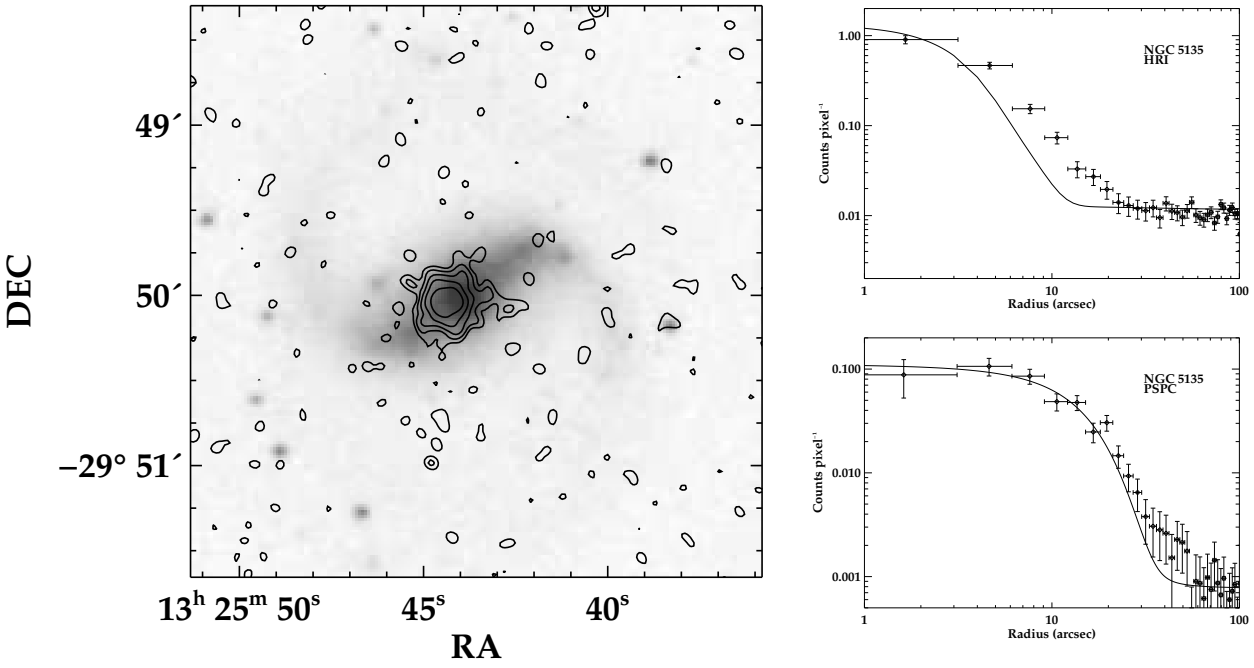

FIG. 1.— Illustration of spatial extent of NGC 5135. (*left*) Contours of *ROSAT* HRI intensity overlaid on the Digitized Sky Survey optical image, where raw X-ray data have been smoothed by a Gaussian of FWHM=4″. The minimum contour level is 3 standard deviations above the background, and contour intervals are logarithmic, in factors of 2. (*right*) Radial profile data points are azimuthal averages of counts per raw (0.″5) pixel. The background and amplitude are fit to the appropriate theoretical point-spread function (*solid line*) for the HRI (*top*) and PSPC (*bottom*). In both cases, NGC 5135 is resolved.

both. Approximately half of this sample contain starbursts, identified by the spectroscopic signatures of luminous young stars, such as stellar wind lines, Balmer absorption, and broad Wolf-Rayet emission features (Heckman et al. 1997; Wang, Heckman, & Lehnert 1997; Cid Fernandes, Storchi-Bergmann, & Schmitt 1998; González Delgado et al. 1998; Schmitt, Storchi-Bergmann, & Cid Fernandes 1999; González Delgado, Heckman, & Leitherer 2000). We restrict our sample to these known Seyfert/starburst composites plus several galaxies that Heckman et al. (1995) had excluded from their study only because IUE had not observed them but which fulfill the original selection criteria. Our sample is unbiased, but we exclude several known composite galaxies that were not part of the original Whittle (1992) compilation. Table 1 contains a summary of the optical and far-infrared (FIR) properties of our sample. Distances are calculated assuming $H_0 = 75\,\mathrm{km\,s^{-1}\,Mpc^{-1}}$ (column 4). Galactic column density, *IRAS* fluxes in four bands, and galaxy inclination are noted columns 6 through 11, respectively.

As described in Paper I, we expect the composite nature of these galaxies to be apparent in their morphologies and spectra. While the spatial signature of an AGN is an unresolved central point source, the Sy2/SBs should also exhibit extended soft X-ray emission. Analogous to nearby starburst galaxies, the collective effect of stellar winds and supernovae drives a hot "superwind" out of the galactic plane (e.g., Chevalier & Clegg 1985, and Heckman, Lehnert, & Armus 1993), which extends to scales of up to tens of kpc. Spectrally, we detect X-rays due to the AGN both directly—though obscured—and indirectly, in scattered light. Both of these continuum components are characterized by a power law of photon index $\Gamma \approx 1.9$, as observed in Seyfert 1 galaxies (Nandra & Pounds 1994), assuming the central engines of Sy 1s and Sy 2s are intrinsically identical. With the addition of a starburst, soft thermal emission ($kT \sim 1$ keV) is also present.

With this physical motivation, we model X-ray images and spectra obtained with *ROSAT* and *ASCA*. The *ROSAT* High Resolution Imager (HRI) provides spatial resolution of about 5″. The *ROSAT* Position Sensitive Proportional Counter (PSPC) provides spatial resolution of about 30″, with higher sensitivity to measure the extremely low surface brightness extended emission better, and some spectral resolution. Data obtained with *ASCA* allow spectroscopy at energies ranging from about 0.5 to 10 keV, which we combine with PSPC spectra when available.

Tables 2 and 3 summarize the results of the model fitting, which we describe in detail in Paper I. We measure the fraction of resolved emission in the HRI and PSPC images two ways. In the first method (Table 2, columns 3 and 6), it is the residual in excess of a single point source, which we model as the instrumental point spread function. This is a conservative estimate, for it usually implies an unfilled ring of extended emission, which is physically unlikely. In the more realistic method (columns 4 and 7), we constrain the residual profile to be flat within the central core of the point spread function. Eleven of the twelve galaxies observed with *ROSAT* exhibit extended emission,

measured by at least one of these methods. As an example, Figure 1 illustrates the spatial extent of NGC 5135 with a *ROSAT* HRI map and radial profiles from both HRI and PSPC observations, which represent the conservative measurement method.

Table 3 contains the parameters of the best-fitting spectral models. In addition to the power laws and thermal emission described above, we also considered including Fe Kα lines near 6.4 keV and provide upper limits on their equivalent widths where the lines are not required. In all cases, the inclusion of additional model components or free parameters is significant at the 90% confidence level, based on an F test. With one exception (Mrk 477), all the twelve galaxies for which we have *ASCA* spectra require a thermal component, with typical $kT = 0.8$ keV, which is characteristic of pure starburst galaxies. For comparison with the imaging results, we list the fraction of soft (0.5–2.0 keV) X-rays that are due to this thermal emission in column 8 of Table 2.

3. RESULTS

3.1. *Synopsis of Paper I*

Based on spectral fits, we find that Seyfert/starburst composite galaxies possess two types of continuum shapes (Figure 2). The first shows a steadily decreasing spectral intensity from low energies to high energies and no clear evidence for a hard X-ray "bump" that would suggest we are seeing a buried AGN directly through large amounts of obscuring matter (e.g., NGC 7130). This spectral type is common to nearby starburst galaxies (Dahlem, Weaver, & Heckman 1998), although in the Sy2/SBs the AGNs also contribute to the hard X-ray flux. The second shows two distinct spectral components: a soft X-ray peak and a hard X-ray peak, consistent with an absorption hump associated with a buried AGN (e.g., Mrk 477). This type is typical of pure, scattering-dominated Seyfert 2 galaxies such as Mrk 348 (Netzer, Turner, & George 1998; Awaki et al. 2000). The observed distribution in spectral types can be produced by varying contributions of an AGN and a starburst, including some examples that contain both the direct and scattered AGN components in addition to the soft X-ray starburst (e.g., Mrk 273). Two members of our sample are exceptional, and these representative spectra do not characterize them well. The complex spectrum of NGC 1068 includes two thermal and three Fe line components in addition to the power law of the scattered AGN. The central source of NGC 6221 is only slightly absorbed. Although a thermal component is present and of comparable luminosity to the other examples, it is weak with respect to the nuclear source.

All the composite galaxies we have observed with *ASCA* except NGC 6221 exhibit a heavily absorbed ($N_H > 10^{23}\,\mathrm{cm}^{-2}$) power-law component, either viewed directly or inferred from other means. In about half the cases, we explicitly model the buried AGN and its scattered soft X-ray emission. In the other examples, the models consist of thermal emission and a single power-law component. We interpret the low foreground column density and lack of a second, absorbed (in the *ASCA* bandpass) power-law component in NGC 1068, Mrk 1066, Mrk 266, and NGC 7130 as evidence that the intrinsic AGN is completely buried and fully absorbed by $N_H \gtrsim 10^{24}\,\mathrm{cm}^{-2}$. *ASCA* observations are not sensitive to such high column densities, and higher-energy data are required to measure the intrinsic power law and absorption accurately in these instances, as well as in NGC 5135. NGC 1068 has been observed with *BeppoSAX*, which is sensitive up to 100 keV, and the broad-band spectrum is consistent with the complete blocking of the intrinsic AGN (Matt et al. 1997). Furthermore, NGC 7674, one of two members of our sample that was not observed with *ASCA*, is observed with *BeppoSAX* to be Compton thick (Malaguti et al. 1998).

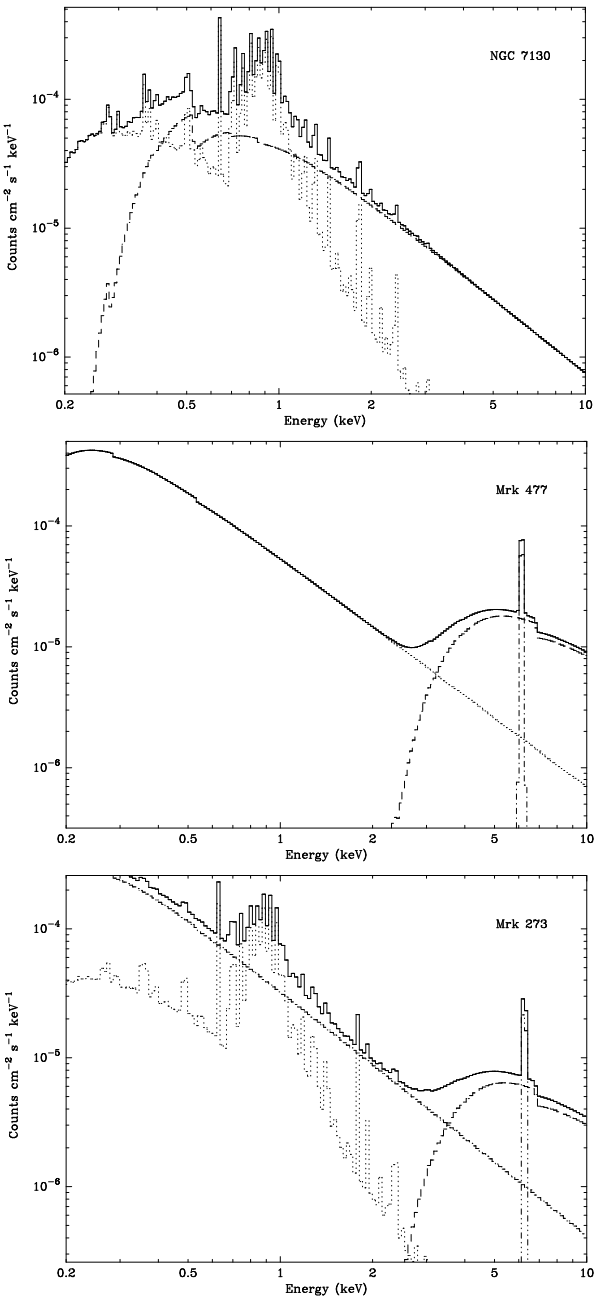

FIG. 2.— Best-fitting model spectra, explicitly revealing the multiple components that comprise them. NGC 7130 and Mrk 477 illustrate the two characteristic continuum shapes of the composite galaxies, depending on whether the intrinsic AGN is completely absorbed, as in the former, or partially emerges to add a high-energy bump, as in the latter. Varying degrees of absorption, scattering, and relative strength of the thermal component (e.g., Mrk 273), account for most variations of the observed spectra.

3.2. *X-ray Properties of the Sample*

Where both the intrinsic and scattered AGN are observed, we estimate how much of the AGN spectrum is scattered into our line of sight by defining a scattering fraction, f_{scatt}, calculated from the ratio of the soft X-ray power law to the hard X-ray (absorbed) power law. The observed f_{scatt} varies from 0.02 to 0.11, with an average of 0.05. The scattered fractions are similar to ordinary Seyfert 2s (Mulchaey et al. 1993) and polarized broad line Sy 2s (Awaki et al. 2000). The scattered fraction does not depend on the column density that absorbs the hard emission; both high and low column densities produce high and low scattered fractions. While broad optical lines have been observed in the polarized light of some sample members, the measured scattering fraction in these instances is moderate, not extreme.

With the exception of Mrk 477, all the preferred models include thermal emission. The temperatures of these thermal components range from 0.16 to 2.3 keV, having a mean $kT = 0.82$ keV. The temperature distribution of the thermal component of the composite galaxies is not significantly different from the moderate temperatures measured in starburst galaxies, as Figure 3 illustrates, comparing with starburst spectra from *ROSAT* and *ASCA* that have been analyzed jointly in the literature.

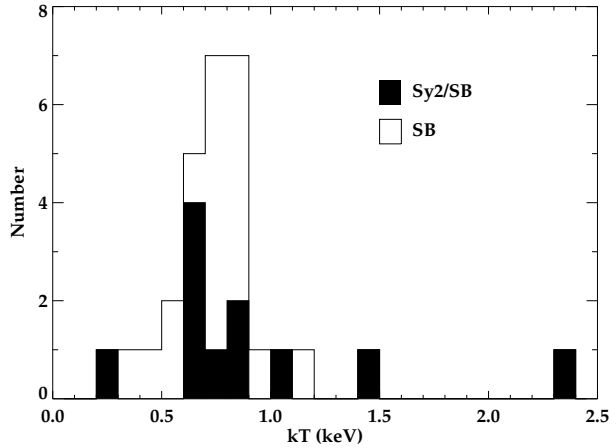

FIG. 3.— Histogram of thermal component temperatures measured in the Sy2/SB sample and the moderate thermal temperatures of ordinary starburst galaxies. The mean temperatures are not significantly different between these two samples, supporting the starburst origin of the thermal component in the composite galaxies. Joint *ROSAT*+*ASCA* spectra were analyzed for the starburst sample, which include: NGC 253, NGC 3029, NGC 3628, NGC 4631, and M82 (Dahlem et al. 1998); NGC 1097, NGC 4736, and M83 (D. K. Strickland 2000, private communication); NGC 1569 (della Ceca et al. 1996); NGC 1808 (Awaki et al. 1996); NGC 2146 (della Ceca et al. 1999); NGC 3256 (Moran, Lehnert, & Helfand 1999); NGC 3310 (Zezas, Georgantopoulos, & Ward 1998); NGC 4038/4039 (Sansom et al. 1996); NGC 4449 (della Ceca, Griffiths, & Heckman 1997); NGC 6240 (Iwasawa 1999); and Arp 299 (Heckman et al. 1999).

The soft X-rays in Mrk 477 are consistent with purely scattered flux from an AGN (Awaki et al. 2000), but the spectrum of Mrk 477 can also be fitted with a thermal component added to the best-fitting scattered power law plus line model. The additional component is not statistically significant and the errors are large, but the best thermal model parameters are reasonable: $kT = 0.9$ keV and $A3 = 9.3 \times 10^{-6}$.

The fluxes listed in Table 3 are the observed quantities. To compare the galaxies, we calculate the corresponding luminosities (Table 4), corrected for absorption by the intervening Galactic column density. Most of the composite galaxies have large amounts of intrinsic absorption, and these absorption corrections can be very uncertain. Therefore, we consider only the emerging hard X-ray luminosity from 2 to 10 keV, $L_{2.0-10}$ or HX, not corrected for the intrinsic column density. We find values of $L_{2.0-10}$ between 9.1×10^{40} and $3.3 \times 10^{42}\,\mathrm{erg\,s^{-1}}$, with a mean $< L_{2.0-10} >= 4.2 \times 10^{41}\,\mathrm{erg\,s^{-1}}$. The total soft X-ray luminosities between 0.5 and 2.0 keV, $L_{0.5-2.0}$ or SX, are corrected for absorption due to our Galaxy. They range from 2.6×10^{40} to $5.6 \times 10^{41}\,\mathrm{erg\,s^{-1}}$, with $< L_{0.5-2.0} >= 1.3 \times 10^{41}\,\mathrm{erg\,s^{-1}}$. In all galaxies except Mrk 477, the total hard and soft luminosities are similar. For comparison, we list the spatially extended and total soft X-ray flux measured with the *ROSAT* HRI and PSPC. The HRI provides no spectral information, and the resolved components alone of the PSPC observations have inadequate signal with which to measure the spectrum directly. Thus, we convert the observed count rates to fluxes adopting an emission model of a thermal plasma at 1 keV with Galactic absorption. The extended fractions are based on the conservative estimates of resolved emission. In Table 4, we also list the medium (0.5-4.5 keV) X-ray luminosities, MX, which we discuss below.

From our spectral decomposition models of power law and thermal emission, we can compare the relative strength of the thermal and scattered components. $SX_{thermal}$ ranges from 0.2 to 1.2 times SX_{scatt}, with an average of 0.6. However, the data are not sensitive enough to search for a correlation. This is partly a selection effect since a weak starburst would not be detected, as in Mrk 477. The fraction of total soft X-ray luminosity due to the thermal component of the best-fitting spectral models is listed in column 8 of Table 2, along with the fraction of extended emission measured in *ROSAT* images.

The spectral and imaging results are generally consistent. The spectral measurement of 100% thermal soft X-ray luminosity in IC 3639 is an overestimate, considering the evidence for some scattered nuclear emission, although it is not statistically significant in the current data. Both imaging methods begin with the assumption that a single point source is an appropriate model for the principal spatial distribution of X-rays. In the examples where the X-ray emission is extremely extended or exhibits a great deal of structure, such as NGC 1068, Mrk 266, and NGC 7582, this assumption is incorrect, and the resulting imaging and spectral fits disagree somewhat.

In several cases with high signal-to-noise ratios, the differences between the softest (0.2–0.4 keV) and harder (0.4-2.0 keV) emission that the PSPC spectrally resolves also supports the identification of extended thermal plasma. Emission in these two broad bands is spatially distinct (Paper I, Figures 5–8). The harder emission tends to be more centrally concentrated, and most of it is due to the AGN directly. The softer flux is more diffuse. Although some of this emission comes from the AGN, more of it is due to the extended component, which we associate with the starburst-driven outflow.

The greatest disagreement between the imaging and

spectroscopic identification of the extended thermal component arises in the obviously variable members of the sample. The *ROSAT* and *ASCA* observations of each of these galaxies, NGC 6221 and NGC 7582, were separated by a year or two. We account for these discrepancies by assuming the intrinsic AGN or its obscuring column density changed and do not require any variation of the extended thermal component itself.

We adopt solar abundances in the spectral models because the data are inadequate to reliably measure the metallicity. Single-temperature thermal plasma models of high-quality spectra of starburst galaxies often require extremely low abundances, however (Dahlem et al. 1998). In these models, with a reduced population of metal ions, the X-ray line emission relative to the continuum is suppressed. The success of the model fits does not necessarily mean that the abundance is genuinely low in the X-ray-emitting region, but rather that the observed line emission is diluted with respect to the continuum, possibly due to the presence of an additional continuum source (Weaver, Heckman, & Dahlem 2000; Strickland & Stevens 2000). In our models of Sy2/SBs, the thermal component represents the net starburst emission. In light of the empirical conclusions in pure starburst galaxies, we examined fixed low abundance ($Z = 0.05 Z_{\odot}$) thermal models in the best-fitting cases. Table 5 summarizes these results in terms of two key parameters: the ratio of intrinsic to scattered AGN continuum, and the fraction of soft emission that is thermal. We apply the low abundance to the best-fitting model and note the quality of this fit (χ^2/dof) in the last column. In general, the low abundance models do not significantly alter the observed scattered fractions, but they tend to increase the proportion of thermal emission. The effects are strongest in Mrk 273, Mrk 463, and NGC 6221, in which the thermal fraction increases significantly and the scattered fraction also decreases measurably. In Mrk 273, in fact, the scattered component is not directly detected in the low abundance model.

4. DISCUSSION

4.1. *Composite X-ray Sources*

All the sample galaxies exhibit X-ray evidence for an AGN, which is consistent with their optical classification as Seyfert 2s. NGC 6221 is unique in that it is the only galaxy that has a truly Seyfert 1-like X-ray spectrum, with a broadened Fe Kα line that suggests origin in an accretion disk (Nandra et al. 1997). The other objects contain a heavily absorbed hard X-ray component consistent with a buried AGN ($N_H > 10^{23}\,\mathrm{cm}^{-2}$), similar to more traditional X-ray selected Seyfert 2s. Where the intrinsic hard X-ray emission is completely absorbed and the AGN is not directly detected, the Fe Kα line emission is consistent with scattered light from an AGN (see Paper I, Figure 12). At high energies, the Sy2/SB composites are indistinguishable from scattering-dominated Seyfert 2s (Netzer et al. 1998; Awaki et al. 2000). The soft X-ray images and spectra, however, are complex. The data require composite energy sources—both an AGN and a starburst—in each case.

4.2. *X-ray Morphology*

The PSPC and HRI images show extended features. Eleven of twelve observed galaxies are extended in the HRI (according to at least one of two measurement techniques) while six of eight are significantly extended in the PSPC. Extended emission is visible to scales as large as about 30 kpc, and the fraction of flux in the extent can make up as much as 80% of the total flux. The presence of extended emission on such large scales rules out the central AGN as the exclusive source of soft X-rays. The most likely sources of soft X-rays are the galaxy disk, AGN-driven jets or winds, and starburst-driven winds. We consider these possibilities in turn, ultimately favoring the starburst origin of extended emission in these composite galaxies.

The fraction of soft X-ray emission that is resolved in images is comparable to the fraction of thermal emission we detect spectroscopically. Thus, we attribute a common origin to the extended soft X-rays and the thermal component. Although the interstellar medium (ISM) of galaxies and AGN outflows share some of these characteristics, overall these extended/thermal components most resemble starburst galaxies in their physical properties, including sizes, temperatures, and X-ray to far-infrared luminosity ratios, as we discuss below.

Normal galaxies emit X-rays. These originate in point sources—including individual stars, X-ray binaries and supernovae—and a hot diffuse component of the ISM, which is the net result of supernova remnants. The total X-ray luminosity of a normal galaxy is generally less than $10^{40}\,\mathrm{erg\,s}^{-1}$ (e.g., Fabbiano 1996), which is significantly smaller than the extended emission we measure in the Sy2/SB sample. Also, for each composite galaxy, the optical and X-ray morphology are distinct. Particularly in the nearby examples, where instrumental resolution is not a significant limitation, we find that the X-ray emission poorly traces the optical disk. Instead, in the nearly face-on cases, it is strongly concentrated near the nucleus, although it is resolved and therefore not due entirely to the AGN. In the edge-on cases, the soft X-rays extend perpendicular to the plane and are not confined to the disk. Thus, normal galactic emission is not the source of the diffuse X-rays in the Sy2/SB sample.

With an outflow or "jet," an AGN can directly generate extended, thermal X-ray emission, shock-heating the ambient material. (We disregard direct generation of non-thermal X-rays in the jet, which would not share the thermal spectral characteristic we observe.) AGN-driven jets exist in nearby radio-quiet AGN on scales as large as a few kpc (Colbert et al. 1996). In Seyfert galaxies, however, AGN-driven outflows tend to be small, having physical scales less than 500 pc (Ulvestad & Wilson 1984) rather than extending to the tens of kpc we observe in these examples. In a small sample of Seyfert galaxies, Baum et al. (1993) observe kpc-scale radio extent and argue that this is due to circumnuclear starbursts, based on the alignment of this emission with the galaxies' minor axes and its misalignment with smaller-scale radio emission.

A radio jet of 500 pc radius is observed in NGC 1068 (Wilson & Ulvestad 1982). This linear radio structure is much smaller than the X-ray extent this galaxy, however, so the extended and thermal X-ray emission of NGC 1068 are not due to the jet. At radio wavelengths, Mrk 78 extends around a central core, linearly toward the east and

in a diffuse lobe toward the west, with associated [O III] emission (Pedlar et al. 1989). The radio size is around $2''$ (1.4 kpc), which is much smaller than the X-ray radius of 20–30 kpc. Another distinction is that while the radio and optical line emission extend east-west, the X-ray emission is wedge-shaped, opening toward the south (Paper I). Mrk 463 is similar to Mrk 78, containing a small ($1'' = 1$ kpc) linear radio structure (Unger et al. 1986; Mazzarella et al. 1991; Kukula et al. 1999) that is associated with [O III] line emission (Uomoto et al. 1993). Mrk 1066 also has a small (300 pc) linear radio jet and coincident [O III] emission (Bower et al. 1995). The northern X-ray structure of Mrk 266 has been called a "jet," but there is no definitive evidence (from kinematics or additional observations at other wavelengths) for this physical origin. Furthermore, even morphologically this identification is suspect, for the emission is not strongly collimated. No AGN-driven outflows have been conclusively identified in any of the other sample members.

The absence of resolved X-ray emission in most ordinary Seyfert 2 galaxies further argues against its AGN origin in the composite objects. Where small-scale radio jets are observed, the X-ray emission is not necessarily resolved (e.g., Mrk 3; Kukula et al. 1993, Morse et al. 1995). No systematic studies of extended X-ray emission in Sy 2s exist, but few of the individual examples that have been examined exhibit the characteristic resolved thermal emission on the large scales we detect in the Sy2/SBs (Colbert et al. 1998). Moreover, several of the exceptional cases that are resolved do have some starburst characteristics (e.g., NGC 4388; Matt et al. 1994, Lehnert & Heckman 1995).

The best explanation for this characteristic emission is the starbursts, which produce large volumes of hot gas in superwinds. Nearby starburst galaxies such as M82 and NGC 253 have kpc-sized X-ray emission from starburst-driven winds (Dahlem et al. 1998), while the starburst-driven X-ray halo of NGC 3628 is even larger, extending 25 kpc (Dahlem et al. 1996). These are comparable to the observed extended X-rays in our sample. In the more inclined examples (Mrk 1066 and Mrk 78), the X-ray halos extend most obviously perpendicular to the planes of the galaxies, as expected from starburst-driven outflows. Furthermore, we have selected the sample to include only galaxies that definitely contain a starburst, so it is certainly an existing energy source in all cases.

4.3. *X-ray and IR Flux Ratios*

We compare this sample of Sy2/SB composite galaxies with starbursts, Seyfert 2s, and Seyfert 1s in order to identify empirical diagnostics of their complex nature. Because the focus of the present work is the composite galaxies, we rely on published comparison samples. These comparison galaxies have not been selected in the same rigorous way as the Sy2/SB sample. The X-ray measurements of Sy 2 and SB galaxies are particularly sensitive to modelling, and we use data that have been analyzed similarly for these two groups. The Sy 1s are least sensitive to modelling because the intrinsic AGN dominates the X-ray emission across the bandpass we examine.

The starbursts consist of the far-infrared flux-limited sample of edge-on galaxies of Dahlem et al. (1998) and the corresponding face-on sample of D. K. Strickland, K. A. Weaver, & T. M. Heckman (in preparation). The Sy 2s are taken from Weaver et al. (2000), which consists of those Seyfert 2 galaxies for which archival *ASCA* observations were available as of 1996 August. This group includes some Sy 2 galaxies that contain starbursts but which are excluded from the present composite sample because they were not compiled in the original (Whittle 1992) list from which Heckman et al. (1995) drew their sample, or because they failed to meet the latter's flux criteria. In subsequent figures, we identify these galaxies (NGC 1667, NGC 1808, NGC 4945, and Circinus) with both the "Sy 2" and "Sy2/SB" symbols. The Sy 1 comparison sample consists of those galaxies compiled by Mas-Hesse et al. (1995) that have measurements of both hard and soft X-ray luminosities. Because of their sample selections, the Sy 2 and Sy 1 groups risk favoring of X-ray-bright sources. With the combination of luminosity ratios and absolute luminosities that we explore, however, this does not appear to be a significant bias.

The X-ray luminosities we consider are in the soft (0.5–2 keV) and hard (2–10 keV) bands, SX and HX, respectively. We correct these for Galactic absorption alone. Note that HX is *not* corrected for the measured intrinsic absorption of each source. The far-infrared emission provides another basis for comparison. The FIR flux is computed from f_{60} and f_{100}, the IRAS 60μm and 100μm flux densities, respectively, measured in Jy, to account for all far-infrared emission; $F_{FIR} = 1.26\times10^{-23}(2.58\times10^{12}f_{60} + 1.0\times10^{12}f_{100})$.

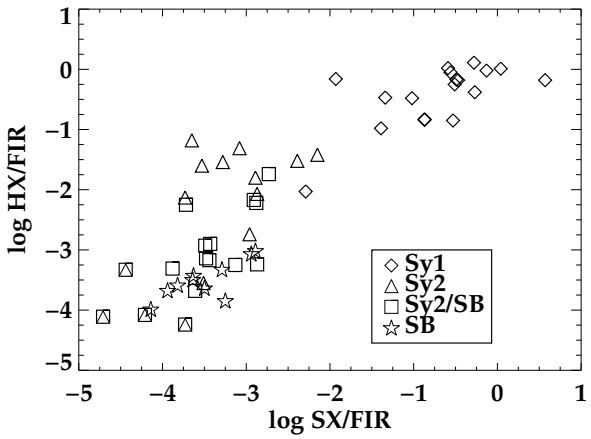

FIG. 4.— Hard (2.0-10 keV) vs. soft (0.5-2.0 keV) X-ray luminosity, normalized by FIR luminosity for the Sy2/SB sample (□), other Sy 2 galaxies (△; Weaver et al. 2000), starburst galaxies (⋆; Dahlem et al. 1998, D. K. Strickland, K. A. Weaver, & T. M. Heckman, in preparation), and Sy 1 galaxies (◇; Mas-Hesse et al. 1995). True composites in the Weaver et al. (2000) sample are plotted with both Sy 2 and Sy2/SB symbols. The composite sample members have SX/FIR ratios similar to starburst galaxies and HX/FIR in between ordinary Sy 2 and starburst galaxies. The Sy 2 examples having relatively low HX/FIR either exhibit significant star formation or are heavily absorbed.

In terms of FIR, the far-infrared luminosity, the ratio of SX/FIR in the Sy2/SB galaxies is similar to that of ordinary starburst galaxies but distinct from those of ordinary Seyfert 2 galaxies. The HX/FIR ratio further separates the Sy2/SBs from Seyfert 2s (Figure 4). As expected, the Sy 2 galaxies of the Weaver et al. (2000) sample that are

known to contain starbursts are spectrally similar to our flux-limited Sy2/SB sample. The composites in which the thermal component is relatively weak are most like other AGN. These sources have a high HX, either due to low absorption, high intrinsic AGN luminosity, or both.

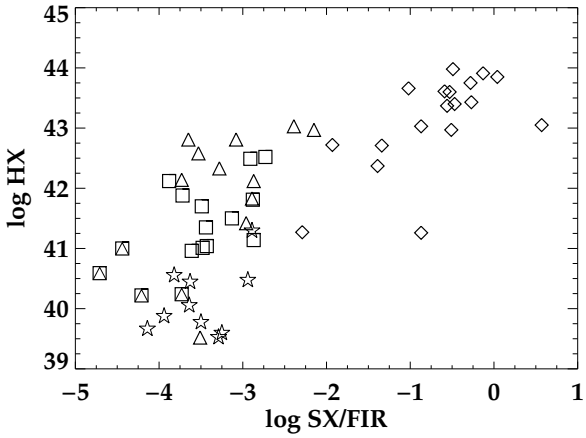

FIG. 5.— The higher observed hard X-ray (2.0-10 keV) luminosities of the Sy2/SB sample distinguish them from starburst galaxies. The strong absorption of nearly all of the composites may account for their relatively low HX with respect to the other Sy 2 galaxies. (Symbols as in Figure 4.)

The hard X-ray luminosity distinguishes the starburst and composite galaxies (Figure 5). A Kolmogorov-Smirnov test demonstrates that HX of the Sy2/SB and SB groups is different to a confidence level greater than 99.9%. We find a maximum hard X-ray luminosity of about $10^{41}\,\mathrm{erg\,s^{-1}}$ for starburst galaxies, while the composites fall between starbursts and Seyfert 2s. These two groups are spectrally similar (e.g., Dahlem et al. 1998), with X-ray binaries, rather than an active nucleus, generating the power-law emission of the starbursts. The central concentration of the X-ray emission, higher luminosities, and the Fe Kα lines of the Sy2/SB examples imply that starburst phenomena alone are not the sole source of X-rays in these objects. Each genuinely contains an active nucleus, as well.

The high X-ray luminosity in both hard and soft bands distinguish the Sy 1s from all the other types we consider. We find $\log(SX/FIR) \gtrsim -2$, $\log(HX) \gtrsim 42.5$, and $\log(HX/FIR) \gtrsim -1$ in the Sy 1s. Comparing SX with the 12μm luminosity, $L12$, we find that the ratio $SX/L12$ does not distinguish the composites from the pure AGNs, but it is a good discriminant of Sy 1s and Sy 2s. In agreement with Rush et al. (1996), all the sources having $\log(SX/L12) > -1$ are Sy 1s, while the active galaxies with $\log(SX/L12) < -2$ tend to be Sy 2s. The ratio $SX/L12$ we observe over the sample of starbursts is similar to the Sy 2s, so this ratio alone is unlikely to be a reliable indicator of the presence of an AGN.

The shapes of the Sy2/SB X-ray spectra strongly depend on the amount of intrinsic absorption, which varies widely across the sample. When N_H is small, we see the AGN shining through (e.g., NGC 7582), while for the heavily absorbed cases (e.g., NGC 5135) the galaxies dominate the spectra. The intrinsic hard X-ray luminosities are sensitive to the models because they depend entirely on correcting for absorption, which is uncertain, especially when N_H is large. Thus, it is difficult to measure the intrinsic physical properties of the AGN. We determine the absorption-corrected hard X-ray luminosity, L^{ac}_{2-10}, to compare our results with others, but we base our conclusions above on the *observed* hard X-ray luminosity from 2 to 10 keV, HX.

The observed hard X-ray luminosity in the Sy2/SBs is somewhat lower than HX measured in other Seyfert 2 galaxies, and the the heavily-absorbed composites are significantly underluminous in observed hard X-rays with respect to Seyfert 1s. If the unified model is correct, in which the Seyfert classification is determined merely by orientation, then we expect Seyfert 2s to have intrinsic hard X-ray properties similar to Seyfert 1s. After correcting for the largest amount of absorption that we can measure with *ASCA*, however, we find that L^{ac}_{2-10} in the composite sample is systematically lower than the hard X-ray luminosity of Sy 1 galaxies. This conclusion holds true even when we ignore the Compton thick sources, those in which we do not observe the AGN directly. Awaki et al. (2000) suggest that polarized broad line Seyferts are underluminous because they are completely blocked. In other words, the observed spectrum is a complex mix of reflected and then absorbed flux. In this case, the true hard X-ray luminosity would be a factor of about 10 higher than the intrinsic flux derived purely from an absorption correction. This would require multiple regions of matter to attenuate and scatter the intrinsic power-law spectrum. If L^{ac}_{2-10} of the composite sample is increased tenfold, the hard X-ray fluxes do become comparable to those of Sy 1s.

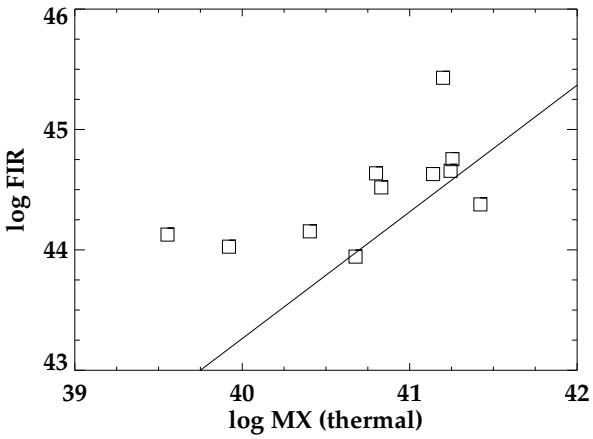

FIG. 6.— Thermal component of medium (0.5-4.5 keV) X-ray luminosity vs. FIR luminosity for Sy2/SB sample (□), corrected for Galactic absorption. The correlation between thermal X-ray and FIR luminosities observed in the composite galaxies agrees with the empirical correlation for normal and starburst galaxies (*solid line*; David et al. 1992). This consistency implies that both are related to star formation processes and are not due to AGNs.

David, Jones, & Forman (1992) determined an empirical relation between the medium X-ray (0.5–4.5 keV) and FIR luminosity for normal and starburst galaxies. The observations of our sample are consistent with this relation. In particular, the FIR luminosity of our sample members follows this relation when *thermal* X-ray luminosity alone—the starburst component—is considered (Figure 6). This

suggests that similar to normal galaxies, the FIR luminosity is related to the stellar activity in the Sy2/SBs. Reprocessed AGN light also adds somewhat to FIR emission, so FIR in the composite galaxies tends to be slightly higher than that associated with the thermal X-ray component alone. For a given FIR luminosity, the *total* medium X-ray luminosity of the Sy2/SBs is consistently greater than expected from the normal and starburst galaxy correlation by factors of several because of the additional AGN contribution to MX. The composites are similar to normal Sy 2s with their high MX_{total}/FIR ratios compared with starburst galaxies (e.g., Green, Anderson, & Ward 1992). Thus, these data imply that similar to normal and starburst galaxies, star formation predominantly determines FIR emission, and the thermal X-ray emission traces this star-forming component.

4.4. *Column Density and Starbursts*

The strength of the fluorescent Fe Kα line is a function of column density. In the Sy2/SBs, we find that the Fe line equivalent widths (EWs) are consistent with simple geometrical scattering models, although we cannot discriminate between them in detail (Paper I, Figure 12). This result requires accurately accounting for intrinsic and scattered continuum flux to identify the large column densities of this sample.

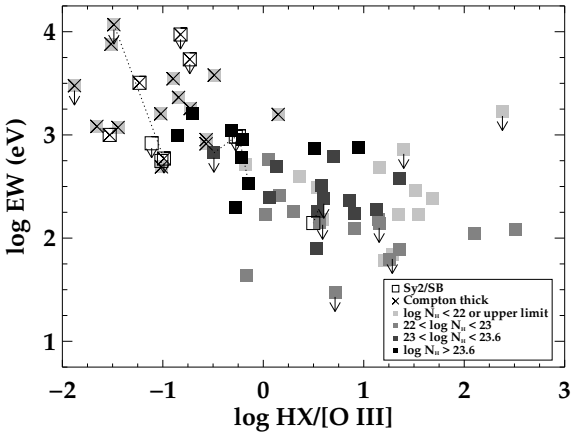

FIG. 7.— Fe K equivalent width vs. hard X-ray/[O III] flux ratio for Sy 2s compiled by Bassani et al. (1999) and our sample of composite galaxies. Measurements of the same source in both works are connected with a dotted line. A large obscuring column suppresses the observed hard X-rays without altering the [O III] flux. The EW is measured with respect to this diminished continuum and is thus relatively large. These effects together help to distinguish the Compton thick sources.

As Bassani et al. (1999) demonstrate empirically for a sample of Sy 2s, the EW combined with the ratio of hard X-ray to [O III] emission is an indicator of N_H. The hard X-ray flux is diminished by the intervening column density, while the isotropic [O III] emission is not directly affected. Increasing N_H thus tends to decrease the ratio HX/[O III]. In the Compton thick regime ($N_H > 10^{24}\,\mathrm{cm}^{-2}$), the emerging continuum at 6.4 keV is suppressed, so the measured EW is therefore relatively large. Indeed, plotting the Sy2/SBs with the Bassani et al. (1999) sample, further illustrates their large column densities (Figure 7).

The distribution of absorbing column density in Sy2/SB composites is significantly different from that measured in "pure" Sy 2s. We compare our sample with the [O III] flux-limited Sy 2 sample of Risaliti, Maiolino, & Salvati (1999), excluding known composites. The two samples are different at the 99% confidence level. The column densities of the Sy 2s with no evidence of a starburst are distributed over a wide range, with 27% having $N_H < 10^{23}\,\mathrm{cm}^{-2}$. In contrast, the Sy2/SBs tend to have higher directly measured or inferred column densities, with $N_H < 10^{23}\,\mathrm{cm}^{-2}$ only in the unusual case of NGC 6221. This result is not a selection effect. The initial sample was flux-limited, based on isotropic AGN properties, and low column densities in these Sy 2s would not affect the optical or UV detectability of the starburst.

The nuclear column densities of molecular gas in ordinary starburst galaxies range from 10^{22} to $10^{25}\,\mathrm{cm}^{-2}$ (e.g., Dahlem et al. 1998, and Kennicutt 1998), and in ultraluminous galaxies, $N_H \sim 10^{23}$ to $10^{25}\,\mathrm{cm}^{-2}$ (Genzel et al. 1998). These column densities are comparable to those measured toward the central engines of Sy 2s. The presence of a dense ISM on circumnuclear scales may explain why the hard nuclear source is generally heavily obscured in the composite objects. Based on the new results from our Sy2/SB sample, we propose that the high inferred X-ray column densities are not solely due to the obscuring torus in these galaxies. *The circumnuclear starburst also obscures the AGN.*

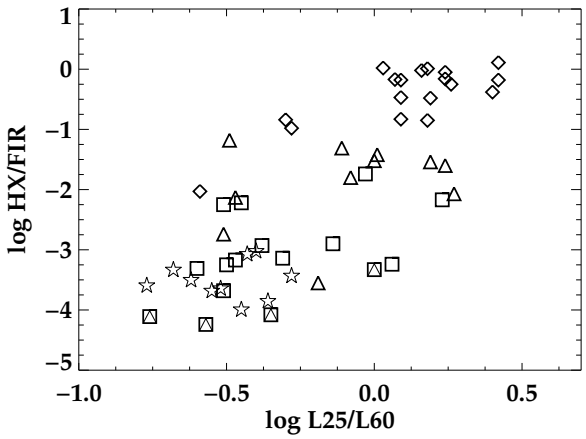

FIG. 8.— Hard X-ray to far-infrared luminosity vs. 25 to 60 μm luminosity for Sy2/SBs and comparison samples. The far-infrared luminosity ratio indicates the relative strength of the AGN and starburst components, with higher values observed when the AGN dominates. The ratio HX/FIR decreases with obscuration. The strong correlation between these two ratios and the absence of many objects from the high-$L25/L60$, low-HX/FIR regime (lower right corner) supports the suggestion that the starburst itself both alters $L25/L60$ and obscures the AGN in composite objects. (Symbols as in Figure 4.)

Comparing the ratio of luminosity at 25 and 60 μm ($L25/L60$) with HX/FIR illustrates the association of starburst activity and obscuration (Figure 8). The ratio $L25/L60$ indicates relative strength of AGN activity compared with star formation, while HX/FIR is a function of obscuration. With increasing obscuration, hard X-rays are blocked, so HX decreases. More material is also available to reprocess the intrinsic emission to the far-infrared band, so FIR increases. As the Sy 1s show, relatively high

values of both of these ratios indicate a relatively strong AGN *and* low obscuration. Including a starburst in an active galaxy not only changes the FIR color, but it also tends to obscure the AGN. Most significantly, few galaxies exhibit high values of $L25/L60$ and low HX/FIR simultaneously. Thus, obscuration of the central engine seems to correlate with the presence of energetically significant star formation. While the comparison samples were not rigorously selected, this correlation is not due to selection effects; heavily obscured and AGN-strong candidates are not preferentially excluded from the comparison groups.

Luminous infrared galaxies ($FIR > 10^{11} L_{\odot}$) exhibit a similar distribution of these flux ratios. To explain these observations, Risaliti et al. (2000) propose that the infrared and X-ray emission suffer different absorption in these galaxies because of a particular viewing geometry. Our results support the suggestion that the X-ray source is more obscured, but it is not a function of viewing angle with respect to the circumnuclear torus. Rather, we specifically identify the starburst, the source of strong 60μm emission, as some of the additional medium that blocks the AGN. A compact torus may still be present, and its orientation may fundamentally account for the classification of these galaxies as Sy 2s rather than Sy 1s, but the torus is not the only absorber.

Observations of bars in Sy 2 galaxies provide further indirect evidence that column density is related to the presence of a starburst. The column density in barred Sy 2s is significantly greater than in non-barred Sy 2s, and more than 80% of the Compton thick Sy 2s are barred (Maiolino, Risaliti, & Salvati 1999). In general, stellar bars are strongly associated with circumnuclear star formation (Kennicutt 1998). Thus, Sy 2s with bars are likely to have high central star formation rates, which we associate with high column density. The physical sizes of obscuration are appropriate, with bar lengths around 100 pc, which is similar to the starburst scales.

The presence of a circumnuclear starburst is a good indicator of large column density. This is true not only in our sample but also in larger samples with different selection criteria, such as Risaliti et al. (1999). In this other sample, we find that many of the heavily obscured active galaxies also contain significant star formation. Because we attribute some of the obscuration to the starburst directly, we suggest that the converse may also hold, that large column density may be a starburst indicator. Indeed, all the Compton thick galaxies of the Risaliti et al. (1999) sample in which the circumnuclear stellar populations have been studied in detail do contain starbursts. Specifically, the column density is measured in 36 members of this sample, and 14 of these are Compton thick. Eight of these 14 have been examined for evidence of starbursts, and all eight show evidence for starbursts. The possible composite nature of the remaining 6 cases is unknown because they have not been examined for indications of star formation.

4.5. *The Role of Galaxy Interactions*

With the exceptions of Mrk 1066 and Mrk 78, all these Sy2/SB composites show evidence for galaxy interactions or mergers. They either contain multiple nuclei, show evidence for interaction with companion galaxies, or are members of groups or clusters. The high incidence of interactions implies that this phenomenon relates to the starburst, probably triggering the star formation, and is therefore important in efficiently providing material to the black hole, either directly—through dynamic instabilities—or indirectly—as a consequence of the starburst winds and supernovae. While the sample numbers are too small to provide statistically significant results, we note that only four of the seven Seyfert 2 galaxies *without* starbursts from the original optical and radio flux-limited sample show evidence for galaxy interactions or mergers or are located in clusters or groups. Starbursts may be important in the complete cycle of development of luminous active galaxies, possibly including the initial creation of the central black hole (Norman & Scoville 1988), through the clearing of obscuring material to allow lines of sight to the AGN directly in type 1 objects at later times (Heckman et al. 1989).

Recent work (Laurikainen & Salo 1995; Dultzin-Hacyan et al. 1999) shows that Seyfert 2 galaxies tend to have more companions than comparison samples of Seyfert 1s and normal galaxies. (In these studies, companions are "nearby" projected onto the plane of the sky, not necessarily physically close.) In particular, Laurikainen & Salo (1995) find that the Sy 2s with companions tend to be morphologically peculiar galaxies. These are most likely to contain starbursts. Seyfert 1s are not preferentially located in denser environments. Because the environment is independent of viewing angle of the AGN and surrounding material, this result challenges the unified model. As we suggest above, the starbursts themselves may literally obscure the unity of the two classes. Interacting galaxies may generate circumnuclear starbursts that obscure the central engine and prevent direct observation of a broad line region. Thus, interacting Seyfert galaxies, a subset of those with companions as defined in large-scale surveys, are more likely to be type 2 than type 1.

5. SUMMARY AND CONCLUSIONS

In this work, we analyze a selection of Seyfert/starburst composite galaxies. These are active galaxies that also contain significant star formation. The sample is flux-limited, based on optical ([O III] $\lambda\lambda 4959 + 5007$) or radio (1.4 GHz) nuclear fluxes, and the starbursts are detected in optical and UV observations.

The results obtained from both X-ray imaging and spectroscopy agree. In the imaging data, we measure fractions of resolved emission that are comparable to the thermal proportions identified in the spectral models. Thus, association of the spatially extended and spectrally thermal emission—common characteristics of starbursts in X-rays—is appropriate. The thermal component generally accounts for a significant fraction of the total soft X-ray emission in these galaxies. The spectra are genuinely complex, and simple models, such as a single power law, that attempt to characterize the intrinsic AGN properties are inapplicable and yield misleading results.

With one exception (NGC 6221), all the AGNs are heavily-absorbed, with $N_H > 10^{23}\,\mathrm{cm}^{-2}$, and the large equivalent widths of the Fe Kα lines are consistent with these high column densities. The column densities of this sample are significantly different from a comparison "pure"

Sy 2 sample. Some fraction of the absorber is likely the starburst itself. We propose that highly obscured AGNs may preferentially contain starbursts. We do not pursue comparisons with Sy 1s because the corrections for intrinsic properties are highly uncertain, but we do note that the total hard X-ray luminosities of the Sy2/SBs are systematically lower than HX of the comparison Sy 1s, even after simple correction for the measured absorption.

The best broad-band discriminant of Seyfert/starburst composites in general samples of galaxies is the ratio of soft X-ray to far-infrared emission, SX/FIR, combined with a hard X-ray measurement. Where it is significant, star formation is ultimately directly tied to much of the soft X-ray and FIR luminosity. These flux ratios of the Sy2/SBs are similar to those of ordinary starburst galaxies, while the AGN produces the hard X-rays. In contrast, pure Sy 2s are more similar to Sy 1s, where nearly all X-ray emission is due to the AGN.

Most of these composite galaxies show signs of interactions or mergers, such as multiple nuclei and membership in groups or clusters demonstrates. This dynamic activity probably triggers star formation, possibly as part of the evolutionary relationship between starburst and Seyfert galaxies. As Heckman et al. (1989) describe, a starburst phase may be one stage in the development of an AGN.

This work was supported by NASA grants NAG5-6917 and NAG5-6400. This research has made use of the NASA/IPAC Extragalactic Database (NED) which is operated by the Jet Propulsion Laboratory, California Institute of Technology, under contract with the National Aeronautics and Space Administration, the Astronomical Data Center at NASA Goddard Space Flight Center, and the High Energy Astrophysics Science Archive Research Center Online Service provided by the NASA Goddard Space Flight Center.

REFERENCES

Adelberger, K. L., & Steidel, C. C. 2000, ApJ, in press (astro-ph/0001126)
Awaki, H., Ueno, S., Koyama, K., Tsuru, T., & Iwasawa, K. 1996, PASJ, 48, 409
Awaki, H., Ueno, S., Taniguchi, Y., & Weaver, K. A. 2000, ApJ, in press (astro-ph/0006054)
Barger, A. J., Cowie, L. L., & Richards, E. A. 2000, AJ, 119, 2092
Bassani, L., Dadina, M., Maiolino, R., Salvati, M., Risaliti, G., della Ceca, R., Matt, G. & Zamorani, G. 1999, ApJS, 121, 473
Baum, S. A., O'Dea, C. P., Dallacassa, D., de Bruyn, A. G., & Pedlar, A. 1993, ApJ, 419, 553
Bower, G., Wilson, A., Morse, J. A., Gelderman, R., Whittle, M., & Mulchaey, J. 1995, ApJ, 454, 106
Chevalier, R. A., & Clegg, A. W. 1985, Nature, 317, 44
Cid Fernandes, R., Jr., Storchi-Bergmann, T., & Schmitt, H. R. 1998, MNRAS, 297, 579
Colbert, E. J. M., Baum, S. A., Gallimore, J. F., O'Dea, C. P., & Christensen, J. A. 1996, ApJ, 467, 551
Colbert, E. J. M., Baum, S. A., O'Dea, C. P., & Veilleux, S. 1998, ApJ, 496, 796
Dahlem, M., Heckman, T. M., Fabbiano, G., Lehnert, M. D., & Gilmore, D. 1996, ApJ, 461, 724
Dahlem, M., Weaver, K. A., & Heckman, T. M. 1998, ApJS, 118, 401
David, L. P., Jones, C., & Forman, W. 1992, ApJ, 388,82
della Ceca, R., Griffiths, R. E., & Heckman, T. M. 1997, ApJ, 485, 581
della Ceca, R., Griffiths, R. E., Heckman, T. M., Lehnert, M. D., & Weaver, K. A. 1999, ApJ, 514, 772
della Ceca, R., Griffiths, R. E., Heckman, T. M., & MacKenty, J. W. 1996, ApJ, 469, 662
Dickey, J. M., & Lockman, F. J. 1990, ARA&A, 28, 215
Dultzin-Hacyan, D., Krongold, Y., Fuentes-Guridi, I., & Marziani, P. 1999, ApJ, 513, L111
Elvis, M., Lockman, F. J., & Wilkes, B. J. 1989, AJ, 97, 777
Fabbiano, G. 1996, in Röntgenstrahlung from the Universe, ed. H. U. Zimmermann, J. E. Trümper, and H. Yorke, (MPE: Garching), 347
Ferrarese, L., & Merritt, D. 2000, ApJ, 539, L9
Gebhardt, K., et al. 2000, ApJ, 539, L13
Genzel, R., et al. 1998, ApJ, 498, 579
Giacconi, R., et al. 2000, submitted to ApJ (astro-ph/0007240)
González Delgado, R. M., Heckman, T., Leitherer, C., Meurer, G., Krolik, J., Wilson, A. S., Kinney, A., & Koratkar, A. 1998, ApJ, 505, 174
González Delgado, R. M., Heckman, T. M., & Leitherer, C. 2000, submitted to ApJ
Green, P. J., Anderson, S. F., & Ward, M. J. 1992, MNRAS, 254, 30
Heckman, T. M., Armus, L., Weaver, K. A., & Wang, J. 1999, ApJ, 517, 130
Heckman, T. M., Blitz, L., Wilson, A. S., Armus, L., & Miley, G. K. 1989, ApJ, 342, 735
Heckman, T. M., Lehnert, M., & Armus, L. 1993, in "The Environment and Evolution of Galaxies," ed. Shull & Thronson (Kluwer: Dordrecht), 455
Heckman, T. M. et al. 1995, ApJ, 452, 549
Heckman, T. M. et al. 1997, ApJ, 482, 114
Hornschemeier, A. E., et al. 2000, ApJ, 541, 49
Iwasawa, K. 1999, MNRAS, 302, 96
Kennicutt, R. C., Jr. 1998, ARA&A, 36, 189
Kukula, M. J., Ghosh, T., Pedlar, A., & Schilizzi, R. T. 1999, ApJ, 518, 117
Kukula, M. J., Ghosh, T., Pedlar, A., Schilizzi, R. T., Miley, G. K., de Bruyn, A. G., & Saikia, D. J. 1993, MNRAS, 264, 893
Laurikainen, E. & Salo, H. 1995, A&A, 293, 683
Lehnert, M. D., & Heckman, T. M. 1995, ApJS, 97, 89
Levenson, N. A., Weaver, K. A., & Heckman, T. M. 2000, submitted to ApJS (Paper I)
Malaguti, G., et al. 1998, A&A, 331, 519
Maiolino, R., Risaliti, G., & Salvati, M. 1999, A&A, 341, L35
Mas-Hesse, J. M., Rodriguez-Pascual, P. M., Sanz Fernandez De Cordoba, L., Mirabel, I. F., Wamsteker, W., Makino, F., & Otani, C. 1995, A&A, 298, 22
Matt, G., et al. 1997, A&A, 325, L13
Matt, G., Piro, L., Antonelli, L. A., Fink, H. H., Meurs, E. J. A., & Perola, G. C. 1994, A&A, 292, L13
Mazzarella, J. M., Soifer, B. T., Graham, J. R., Neugebauer, G., Matthews, K., & Gaume, R. A. 1991, AJ, 102, 1241
Miyoshi, M., Moran, J., Herrnstein, J., Greenhill, L., Nakai, N., Diamond, P., & Inoue, M. 1995, Nature, 373, 127
Moran, E. C., Lehnert, M. D., & Helfand, D. J. 1999, ApJ, 526, 649
Morse, J. A., Wilson, A. S., Elvis, M., & Weaver, K. A. 1995, ApJ, 439, 121
Mulchaey, J. S., Colbert, E., Wilson, A. S., Mushotzky, R. F.,& Weaver, K. A. 1993, ApJ, 414, 144
Murphy, E. M., Lockman, F. J., Laor, A., & Elvis, M. 1996, ApJS, 105, 369
Mushotzky, R. F., Cowie, L. L., Barger, A. J., & Arnaud, K. A. 2000, Nature, 404, 459
Nandra, K., George, I. M., Mushotzky, R. F., Turner, T. J., & Yaqoob, T. 1997, ApJ, 477, 602
Nandra, K., & Pounds, K. A. 1994, MNRAS, 268, 405
Netzer, H., Turner, T. J., & George, I. M. 1998, ApJ, 504, 680
Norman, C., & Scoville, N. 1988, ApJ, 332, 124
Pedlar, A., Meaburn, J., Axon, D. J., Unger, S. W., Whittle, D.M., Meurs., E. J. A., Guerrine, N., & Ward, M. J. 1989, MNRAS, 238, 863
Ridgway, S., Heckman, T., Calzetti, D., & Lehnert, M. 2000, submitted to ApJ
Risaliti, G., Gilli, R., Maiolino, R., & Salvati, M. 2000, A&A, 357, 13
Risaliti, G., Maiolino, R., & Salvati, M. 1999, ApJ, 522, 157
Rush, B., Malkan, M. A., Fink, H. H., & Voges, W. 1996, ApJ, 471, 190
Sansom, A. E., Dotani, T., Okada, K., Yamashita, A., & Fabbiano, G. 1996, MNRAS, 281, 48
Schmitt, H. R., Kinney, A. L., Storchi-Bergmann, T., & Antonucci, R. 1997, ApJ, 477, 623
Schmitt, H. R., Storchi-Bergmann, T., & Cid Fernandes, R. 1999, MNRAS, 303, 173
Strickland, D. K., & Stevens, I. R. 2000, MNRAS, 314, 511
Tanaka, Y., et al. 1995, Nature, 375, 659

Ulvestad, J. S., & Wilson, A. S. 1984, ApJ, 285, 439
Unger, S. W., Pedlar, A., Booler, R. V., & Harrison, B. A. 1986, MNRAS, 219, 387
Uomoto, A., Caganoff, S., Ford, H. C., Rosenblatt, E. I., Antonucci, R. R. J., Evans, I. N., & Cohen, R. D. 1993, AJ, 105, 1308
Wang, J., Heckman, T. M., & Lehnert, M. D. 1997, ApJ, 491, 114
Weaver, K. A., Awaki, H., Mulchaey, J. S., Colbert, E. J. M., Yaqoob, T., & Ueno, S. 2000, submitted to ApJ
Weaver, K. A., Heckman, T. M., & Dahlem, M. 2000, ApJ, 534, 684
Whittle, M. 1992, ApJS, 79, 49
Wilson, A. S., & Ulvestad, J. S. 1982, ApJ, 263, 576
Zezas, A. L., Georgantopoulos, I., & Ward, M. J. 1998, MNRAS, 301, 915

Table 1

Basic Properties of the Selected Galaxies

Galaxy	RA (h	m	s)	DEC (°	′	″)	D (Mpc)	Scale (pc/″)	Galactic N_H (10^{20} cm^{-2})	F_{12} (Jy)	F_{25} (Jy)	F_{60} (Jy)	F_{100} (Jy)	i (°)	References
NGC 1068	02	42	40.71	−00	00	47.8	15.2	74	3.0	39.7	85.0	176	224	32	1, 4
Mrk 1066	02	59	58.59	+36	49	14.3	48	233	12	0.45	2.26	11.0	12.1	54	2, 4, 6
Mrk 1073	03	15	01.43	+42	02	09.4	93	452	1.1	0.44	1.41	8.17	11.1	42	2, 5, 6
Mrk 78	07	42	41.73	+65	10	37.5	149	720	4.1	0.13	0.55	1.11	1.13	60	2, 4, 6
IC 3639	12	40	52.88	−36	45	21.5	44	212	5.1	0.64	2.26	7.52	10.7	34	2, 5, 7
NGC 5135	13	25	43.97	−29	50	02.3	55	266	4.7	0.64	2.40	16.9	28.6	46	2, 4, 7, 8, 9
Mrk 266	13	38	17.69	+48	16	33.9	111	540	1.5	0.23	0.98	7.34	11.1	···	1, 4, 10
Mrk 273	13	44	42.11	+55	53	12.6	151	732	0.97	0.24	2.28	21.7	21.4	···	1, 5, 6
Mrk 463	13	56	02.87	+18	22	19.5	199	963	2.1	0.51	1.58	2.18	1.92	10	2, 5, 6
Mrk 477	14	40	38.11	+53	30	16.0	151	733	1.3	0.13	0.51	1.31	1.85	···	2, 5, 7, 11
NGC 6221	16	52	46.67	−59	12	59.0	20	96	15	1.49	5.27	36.3	84.5	43	2, 5, 8
NGC 7130	21	48	19.48	−34	57	09.2	65	313	2.0	0.59	2.12	16.5	25.6	29	2, 5, 7, 8, 9
NGC 7582	23	18	23.50	−42	22	14.0	21	102	1.5	1.62	6.44	49.1	72.9	62	3, 5, 8, 9
NGC 7674	23	27	56.72	+08	46	44.5	116	563	5.2	0.67	1.90	5.59	8.15	25	2, 4, 6

References. — (1) Murphy et al. 1996; (2) Dickey & Lockman 1990; (3) Elvis, Lockman, & Wilkes 1989; (4) Schmitt et al. 1997; (5) Whittle 1992; (6) González-Delgado et al. 2000; (7) González-Delgado et al. 1998; (8) Cid Fernandes et al. 1998; (9) Schmitt et al. 1999; (10) Wang et al. 1997; (11) Heckman et al. 1997

TABLE 2
EXTENDED AND THERMAL SOFT X-RAY EMISSION

	HRI			PSPC			ASCA
Galaxy	R^{a}_{kpc}	f^{b}	f^{c}	R^{a}_{kpc}	f^{b}	f^{c}	f^{d}_{therm}
NGC 1068	7.4	$0.51^{+0.05}_{-0.09}$	0.73 ± 0.02	7.4	0.40 ± 0.02	0.60 ± 0.06	0.80
Mrk 1066	0.0	< 0.15	< 0.71	...	...	...	0.51
Mrk 1073	9.5	$0.53^{+0.18}_{-0.28}$	$0.84^{+0.16}_{-0.50}$	...	...	...	0.91
Mrk 78	17	$0.38^{+0.20}_{-0.30}$	$0.72^{+0.28}_{-0.54}$	36	< 0.62	$0.72^{+0.28}_{-0.45}$	...
IC 3639	6.8	$0.39^{+0.11}_{-0.21}$	0.68 ± 0.31	...	...	...	1.00
NGC 5135	5.3	$0.46^{+0.06}_{-0.16}$	0.65 ± 0.20	13	$0.19^{+0.07}_{-0.11}$	< 0.32	0.54
Mrk 266	22	$0.78^{+0.06}_{-0.16}$	$0.92^{+0.08}_{-0.20}$	32	$0.49^{+0.08}_{-0.12}$	$0.77^{+0.23}_{-0.28}$	0.43
Mrk 273	18	< 0.39	$0.53^{+0.47}_{-0.49}$	37	< 0.28	< 0.62	0.43
Mrk 463	...	...	...	48	< 0.41	< 0.67	0.31
Mrk 477	15	< 0.30	0.54 ± 0.35	...	...	...	0.00
NGC 6221	4.8	$0.52^{+0.07}_{-0.17}$	$0.96^{+0.04}_{-0.22}$	...	...	...	0.05
NGC 7130	16	$0.44^{+0.23}_{-0.33}$	< 0.63	...	...	...	0.57
NGC 7582	3.1	$0.56^{+0.09}_{-0.19}$	$0.94^{+0.06}_{-0.27}$	5.1	$0.38^{+0.08}_{-0.12}$	0.54 ± 0.28	0.16, 0.28
NGC 7674	...	...	...	45	$0.65^{+0.48}_{-0.52}$	< 0.57	...

[a]Maximum radius of extended emission (kpc).

[b]Minimum extended fraction of total emission, with 90% confidence errors.

[c]Constrained measurement of extended fraction of total emission.

[d]Thermal fraction of soft emission in spectrum.

TABLE 3

BEST-FITTING MODELS ($\Gamma = 1.9$)

	Hard Component						Soft Component					
Galaxy	N_H^a	$A1^b$	E_{line}^c	σ_{line}^d	EW_{line}^e	F_{2-10}^f	N_H^a	$A2^g$	kT^h	$A3^i$	$F_{0.5-2}^j$	χ^2/dof
ASCA												
NGC 1068	...	...	$6.4^{+0.03}_{-0.06}$	0.05f	1000^{+260}_{-630}	49 ± 1.7	3.0f	$9.0^{+0.50}_{-0.56}$	0.69 ± 0.02	$18^{+0.39}_{-0.77}$	64.2 ± 3.2	1870/786
	...	...	$6.6^{+0.07}_{-0.06}$	0.50f	4200^{+500}_{-630}	...	...	...	1.66 ± 0.2	$7.6^{+1.6}_{-1.3}$	...	...
	...	...	$6.7^{+0.24}_{-0.08}$	0.05f	350^{+150}_{-190}	...	...	...	...	...	...	...
Mrk 1066	$57^{+59}_{-45:}$	$0.97^{+0.25}_{-0.29}$	$6.6^{+0.20}_{-0.52}$	0.05f	3200 ± 1900	3.6 ± 0.47	12f	...	$0.88^{+0.22}_{-0.20}$	$0.42^{+0.14}_{-0.11}$	1.3 ± 0.17	74/73
Mrk 1073	400^{+390}_{-220}	$2.2^{+0.89}_{-0.70}$	...	...	...	$4.7^{+0.74}_{-0.85}$	14f	...	$1.0^{+0.47}_{-0.29}$	$0.70^{+0.82}_{-0.28}$	1.3 ± 0.26	119/63
IC 3639	2100^{+3000}_{-1300}	$3.4^{+3.2}_{-1.7}$	...	...	< 830	4.8 ± 1.2	5.1f	...	$2.3^{+2.9}_{-0.7}$	1.7 ± 0.53	1.2 ± 0.29	48/53
NGC 5135	12900^{+16000}_{-6800}	26^{+120}_{-18}	...	...	< 1100	$6.2^{+1.5}_{-1.6}$	4.7f	$0.67^{+0.09}_{-0.15}$	$0.77^{+0.04}_{-0.1}$	$0.79^{+0.28}_{-0.14}$	$2.8^{+0.5}_{-0.2}$	108/98
Mrk 266	160^{+330}_{-150}	$1.2^{+1.1}_{-0.6}$	...	...	< 10000	3.1 ± 1.1	1.5f	...	0.78 ± 0.3	$0.73^{+0.35}_{-0.39}$	1.8 ± 0.6	13/33
Mrk 273	3300^{+2900}_{-1100}	$3.9^{+2.3}_{-1.9}$	$6.5^{+0.21}_{-0.17}$	0.05f	860^{+130}_{-230}	5.2 ± 1.0	1.0f	$0.48^{+0.14}_{-0.21}$	$1.1^{+0.88}_{-0.77}$	$0.19^{+0.41}_{-0.17}$	1.2 ± 0.24	55/57
Mrk 463	2900^{+1700}_{-1200}	$6.0^{+4.7}_{-2.8}$	...	...	< 890	6.6 ± 1.3	2.1f	$0.40^{+0.080}_{-0.086}$	$0.71^{+0.53}_{-0.45}$	$0.15^{+0.080}_{-0.11}$	1.1 ± 0.17	80/70
Mrk 477	2400^{+1700}_{-1200}	$8.8^{+8.9}_{-4.3}$	$6.4^{+0.23}_{-0.21}$	0.05f	560^{+560}_{-500}	$12^{+2.3}_{-1.9}$	1.3f	$0.59^{+0.22}_{-0.20}$	...	...	1.2 ± 0.2	36/104
NGC 6221	$110^{+8.6}_{-8.3}$	$46^{+1.9}_{-1.3}$	$6.6^{+0.31}_{-0.29}$	0.50f	360^{+210}_{-93}	140 ± 4.1	15f	$3.0^{+1.4}_{-1.5}$	$1.4^{+1.6}_{-0.5}$	$1.2^{+1.7}_{-0.69}$	24 ± 0.7	799/765
NGC 7130	$16^{+62}_{-14:}$	0.60 ± 0.3	...	...	< 5400	1.8 ± 0.3	2.0f	...	$0.79^{+0.2}_{-0.1}$	$0.56^{+0.29}_{-0.25}$	$2.0^{+0.3}_{-0.4}$	74/74
NGC 7582 (1994)	1100^{+74}_{-78}	$84^{+6.6}_{-6.5}$	$6.2^{+0.17}_{-0.33}$	0.05f	190^{+60}_{-140}	140 ± 7.1	1.5f	$2.0^{+0.33}_{-0.30}$	...	...	$4.4^{+0.6}_{-0.5}$	344/284
NGC 7582 (1996)	1400^{+60}_{-50}	$93^{+4.6}_{-4.4}$	6.3 ± 0.08	0.05f	150^{+53}_{-51}	140 ± 4.2	1.5f	$2.1^{+0.14}_{-0.16}$	...	...	$4.4^{+0.2}_{-0.3}$	516/467
ASCA + PSPC												
NGC 1068	...	...	6.4 ± 0.05	0.05f	1000 ± 310	50 ± 2.5	3.0f	$11^{+0.27}_{-0.29}$	0.79 ± 0.01	$18^{+0.55}_{-0.46}$	100 ± 5.0	2315/910
	...	...	6.6 ± 0.07	0.50f	3500^{+250}_{-390}	...	...	...	0.13 ± 0.005	$110^{+9.2}_{-7.9}$	...	...
	...	...	$6.7^{+0.10}_{-0.14}$	0.05f	530^{+410}_{-280}	...	...	...	...	...	...	...
NGC 5135	14000^{+16000}_{-3700}	29^{+100}_{-21}	...	...	< 590	6.3 ± 0.63	4.7f	$0.71^{+0.11}_{-0.10}$	$0.68^{+0.14}_{-0.06}$	$0.79^{+0.10}_{-0.11}$	2.9 ± 0.29	150/119
Mrk 266	$1.5 :^{+1.1}_{-0:}$	0.75 ± 0.2	...	...	< 9400	$2.1^{+0.4}_{-0.8}$	1.5f	...	$0.28^{+0.1}_{-0.05}$	$0.72^{+0.42}_{-0.33}$	$2.6^{+0.5}_{-0.9}$	43/50
Mrk 273	2500^{+1500}_{-890}	$3.2^{+2.9}_{-1.4}$	$6.5^{+0.21}_{-0.17}$	0.05f	970^{+630}_{-680}	4.8 ± 0.91	1.0f	$0.35^{+0.082}_{-0.097}$	$0.84^{+0.48}_{-0.24}$	$0.28^{+.17}_{-0.097}$	$1.3^{+0.15}_{-0.19}$	90/68
Mrk 463	2800^{+1300}_{-850}	$5.8^{+5.0}_{-2.7}$	...	...	< 960	6.6 ± 1.3	2.1f	$0.40^{+0.085}_{-0.094}$	$0.66^{+0.35}_{-0.39}$	$0.16^{+0.086}_{-0.084}$	1.1 ± 0.17	96/87
NGC 7582 (1994)	1000 ± 70	$84^{+6.4}_{-5.9}$	$6.2^{+0.18}_{-0.36}$	0.05f	160^{+100}_{-84}	$140^{+6.9}_{-6.1}$	$5.3^{+5.7}_{-1.6}$	$1.5^{+0.44}_{-0.32}$	$0.46^{+0.32}_{-0.19}$	$0.56^{+0.61}_{-0.32}$	$4.10^{+0.9}_{-1.0}$	365/297
NGC 7582 (1996)	1400 ± 50	$93^{+4.6}_{-4.2}$	6.3 ± 0.08	0.05f	140^{+55}_{-48}	$140^{+4.3}_{-4.0}$	$5.6^{+3.4}_{-1.4}$	1.9 ± 0.20	$0.60^{+0.24}_{-0.30}$	$0.32^{+0.16}_{-0.17}$	4.2 ± 0.4	538/480

[a] Column density in units of $10^{20}\,\mathrm{cm}^{-2}$.

[b] Normalization of power law in units of 10^{-4} photons $\mathrm{keV}^{-1}\,\mathrm{cm}^{-2}\,\mathrm{s}^{-1}$ at 1 keV.

[c] Energy of line center in keV.

[d] Line width in keV.

[e] Equivalent width of line in eV.

[f] 2.0–10.0 keV model flux in SIS0 detector in units of $10^{-13}\,\mathrm{erg\,cm}^{-2}\,\mathrm{s}^{-1}$.

[g] Normalization of the soft power-law component in units of 10^{-4} photons $\mathrm{keV}^{-1}\,\mathrm{cm}^{-2}\,\mathrm{s}^{-1}$ at 1 keV.

[h] Temperature of thermal plasma in keV.

[i] Normalization of thermal component in units of $10^{-4} \times K$, where $K = (10^{-14}/(4\pi D^2)) \int n_e n_H\, dV$, D is the distance to the source (cm), n_e is the electron density (cm^{-3}), and n_H is the hydrogen density (cm^{-2}).

[j] 0.5–2.0 keV model flux in SIS0 detector in units of $10^{-13}\,\mathrm{erg\,cm}^{-2}\,\mathrm{s}^{-1}$.

Note. — Power law photon index is fixed at 1.9. Additional fixed parameters are marked with f. Errors are 90% confidence limits for two interesting parameters, except fluxes, where errors are 90% confidence for one parameter. Parameters that are constrained by hard limits are marked with a colon.

TABLE 4
X-RAY LUMINOSITY

	HRI		PSPC		ASCA				
Galaxy	Extended SX[a]	Total SX[b]	Extended SX[a]	Total SX[b]	Thermal SX[c]	Total SX[b]	Thermal MX[d]	Total MX[e]	HX[f]
NGC 1068	41.4	41.7	41.3	41.7	41.4	41.5	41.4	41.6	41.1
Mrk 1066	<39.8	40.6	···	···	40.5	40.7	40.4	40.9	41.0
Mrk 1073	40.7	41.0	···	···	41.1	41.1	41.1	41.5	41.7
Mrk 78	41.1	41.5	<41.2	41.4	···	···	···	···	···
IC 3639	40.1	40.5	···	···	40.5	40.5	40.7	40.8	41.0
NGC 5135	40.8	41.2	40.5	41.2	40.8	41.1	40.8	41.2	41.4
Mrk 266	41.6	41.7	41.4	41.7	41.3	41.6	41.3	41.8	41.5
Mrk 273	<41.0	41.4	<40.8	41.4	41.2	41.6	41.2	41.8	42.1
Mrk 463	···	···	<41.5	41.9	41.2	41.7	41.2	42.0	42.5
Mrk 477	<41.2	41.8	···	···	···	41.5	···	41.9	42.5
NGC 6221	40.5	40.8	···	···	39.9	41.1	39.9	41.6	41.8
NGC 7130	40.8	41.1	···	···	40.8	41.0	40.8	41.2	41.0
NGC 7582	40.1	40.3	39.9	40.3	39.9	40.4	39.6	41.2	41.9
NGC 7674	···	···	41.3	41.5	···	···	···	···	···

[a]Extended soft X-ray luminosity (0.5-2.0 keV), corrected for Galactic absorption.

[b]Total soft X-ray luminosity (0.5-2.0 keV), corrected for Galactic absorption.

[c]Thermal soft X-ray luminosity (0.5-2.0 keV), corrected for Galactic absorption.

[d]Thermal medium X-ray luminosity (0.5-4.5 keV), corrected for Galactic absorption.

[e]Total medium X-ray luminosity (0.5-4.5 keV), corrected for Galactic absorption.

[f]Total observed hard X-ray luminosity (2.0-10 keV).

Note. — All quantities are log erg s^{-1}.

TABLE 5
METALLICITY EFFECTS

Galaxy	f_{scatt} $Z = Z_\odot$	f_{scatt} $Z = 0.05Z_\odot$	f^{a}_{therm} $Z = Z_\odot$	f^{a}_{therm} $Z = 0.05Z_\odot$	χ^2/dof $Z = 0.05Z_\odot$
NGC 1068	···	···	0.80	0.81	2902/908
Mrk 1066	···	···	0.51	0.86	75/73
Mrk 1073	···	···	0.91	0.98	118/63
IC 3639	···	···	1.00	1.00	52/53
NGC 5135	0.02	0.03	0.54	0.76	135/119
Mrk 266	···	···	0.43	0.94	29/49
Mrk 273	0.11	···	0.43	1.00	94/69
Mrk 463	0.07	0.10	0.31	0.35	102/90
Mrk 477	0.07	···	0.00	···	···
NGC 6221	0.07	0.01	0.05	0.22	798/765
NGC 7130	···	···	0.57	0.57	75/74
NGC 7582 (1994)	0.02	0.02	0.16	0.27	362/296
NGC 7582 (1996)	0.02	0.02	0.28	0.22	541/479

[a]Thermal fraction of soft emission.